Dalton Transactions

ROYAL SOCIETY OF CHEMISTRY

PERSPECTIVE

View Article Online
View Journal | View Issue

Cite this: *Dalton Trans.*, 2026, **55**, 2788

Recent progress in supramolecular coordination complexes for bacterial diagnosis and treatment

Qiao Song,†[a,b] Junhua Zhang,†[b] Lulu Yan,†[b] Zhipeng Zhang,*[a] Junrong Li,*[b] Weiyong Liu*[e] and Yao Sun *[c,d,f]

Received 9th November 2025,
Accepted 26th December 2025

DOI: 10.1039/d5dt02682b

rsc.li/dalton

Bacterial infections are exacerbated by antibiotic resistance and biofilm formation, posing a serious threat to global health. At present, treatment methods that mainly rely on antibiotics are increasingly challenged by antibiotic resistance, and thus innovative solutions are needed. Supramolecular coordination complexes (SCCs) assembled from organic ligands and metal receptors are a promising type of antibacterial agent. SCCs have demonstrated significant application value in the biomedical field, especially achieving remarkable results in tumor treatment and medical imaging diagnosis. Although research on the antibacterial applications of SCCs is still in its early stages, their well-defined antibacterial mechanisms and designable molecular frameworks provide strong potential for addressing drug-resistant bacterial infections. As systematic reviews of the molecular design and mechanisms of SCCs are still scarce, this article reviews the antibacterial mechanisms and design strategies of SCCs, aiming to guide the molecular engineering of advanced antibacterial materials and address the urgent need for effective alternatives to traditional antibiotics.

1. Introduction

Bacterial infections, particularly with the rapid rise of antibiotic-resistant strains, remain a major global public health threat. Currently, bacterial infection treatments primarily rely on antibiotics, which inhibit bacterial growth or kill bacteria, playing a key role in managing various infections.[1,2] However, the extensive use of antibiotics has led to an increasingly prominent issue of antimicrobial resistance (AMR), posing new challenges to therapeutic approaches.[3] According to the World Health Organization (WHO), by 2050, annual deaths caused by bacterial resistance will increase by 67.5%, reaching 1.91 million.[4,5] AMR has become a significant threat to global public health, which is exacerbated by the formation of microbial biofilms that play a crucial role in the evolution and spread of drug-resistant bacteria.[5–7] Biofilms are complex bacterial communities that form on surfaces and are encased in extracellular polymeric substances (EPS).[8–10] Bacteria in biofilms enhance their resistance to antibiotics through the protective matrix formed by EPS, making infection treatment more challenging.[11–13]

In recent years, emerging antibacterial agents mainly include natural materials (such as silver and chitosan), metal-organic frameworks (MOFs),[14,15] covalent organic frameworks (COFs),[16–18] organic small molecules,[19–21] and nanomaterials.[22,23] Most of these agents exert antibacterial effects through chemical and physical methods, yet they still face limitations despite their respective advantages in killing bacteria.[24] For instance, some nanomaterials exhibit broad-spectrum antibacterial activity by disrupting the bacterial membranes and generating reactive oxygen species (ROS).[25–28] Similarly, certain materials with an ideal shape and size, as well as a cationic framework with precisely positioned charges, can interact with bacterial lipid membranes through their inherent properties to form transmembrane channels, effectively disrupting the integrity of bacterial cell membranes.[29–31] Due to the complexity of the bacterial environment and the protection offered by tenacious biofilms, it is difficult to achieve satisfactory outcomes with current clinical diagnosis and treatment.[32,33] Therefore, developing novel drugs that effectively combat antibiotic resistance and disrupt biofilms has become an urgent global public health priority.

Consequently, researchers have focused their attention on supramolecular coordination complexes (SCCs), which are materials precisely assembled from organic ligands and metal acceptors (Scheme 1).[34–36] At present, SCCs have been widely applied in the biomedical field, especially achieving remarkable progress in tumor treatment and imaging.[37–41] Although

[a]*Xianning Medical College, College of Pharmacy, Hubei University of Science & Technology, Xianning 437100, China. E-mail: zzplbeckham@foxmail.com*
[b]*College of Chemistry, Central China Normal University, Wuhan 430079, China. E-mail: Junrong.li@ccnu.edu.cn*
[c]*College of Biomedicine and Health, Huazhong Agricultural University, Wuhan 430070, China. E-mail: sunyaogbasp@mail.hzau.edu.cn*
[d]*Hubei Jiangxia Laboratory, Wuhan 430200, China*
[e]*Department of Laboratory Medicine, Tongji Hospital, Tongji Medical College, Huazhong University of Science and Technology, Wuhan, 430030 Hubei, China*
[f]*Wuhan National Laboratory for Optoelectronics, Huazhong University of Science and Technology, Wuhan, China*
†These authors contributed equally.

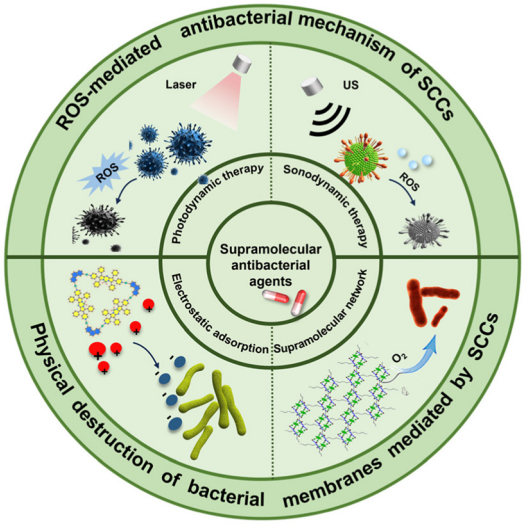

Scheme 1 A Review of the application of supramolecular coordination complexes in bacterial diagnosis and treatment.

their application in the field of antibacterial technology is still in its infancy, its huge potential cannot be ignored. This technology enables targeted design against unique bacterial structures (such as peptidoglycan cell walls/outer membranes) and responds to specific bacterial microenvironmental conditions (*e.g.*, specific enzymes, acidic pH, *etc.*), thereby achieving precise and efficient treatment of drug-resistant bacteria and biofilm infections.[42,43] Additionally, they demonstrates significantly higher selectivity and lower toxicity advantages. SCCs can generate increased levels of ROS, thereby effectively damaging bacterial cell walls or membranes.[44,45] The antibacterial efficacy can be further modulated by varying the types of organic ligands and metal acceptors. For instance, some researchers employ photosensitizers capable of ROS generation under light irradiation as self-assembly ligands, or introduce heterometallic acceptors to obtain highly positively charged SCCs, which enhances membrane interactions and improves antibacterial activity.[46] There are relatively few reviews on the correlation analysis of the specific mechanisms and molecular designs of SCCs' antibacterial properties. Therefore this paper conducts an in-depth analysis of two key antibacterial mechanisms of SCCs – the antibacterial effect of ROS and the antibacterial effect of physical destruction, aiming to explore effective molecular design strategies, lay the foundation for molecular engineering, and promote the research and development of advanced antibacterial materials.

2. Mechanism-oriented design and structure-activity study of antibacterial agents based on SCCs

2.1 ROS-mediated antibacterial mechanism of SCCs

Reactive oxygen-mediated bacterial membrane damage is one of the main mechanisms of action of current antibacterial materials based on SCCs.[47] For instance, singlet oxygen ($^1O_2$) or hydroxyl radicals ($^{\cdot}OH$) can damage membrane lipids, DNA or proteins, thereby leading to irreversible bacterial death. Researchers usually use different photosensitizers or sonosensitizers as ligands for SCCs to generate more ROS.[48–50]

Photodynamic inactivation (PDI) is a novel antibacterial therapy that utilizes photosensitizers to generate ROS (such as $^1O_2$) under light exposure, exerting bactericidal effects by destroying key molecules such as bacterial membranes and DNA.[51] At present, the optimal design of photosensitizers is the research focus for improving the efficiency of PDI. Traditional photosensitizers currently face the issue of aggregation-caused quenching (ACQ).[52–54] When these photosensitizers aggregate, fluorescence self-quenching occurs, and their ability to generate ROS significantly decreases, greatly limiting their effectiveness in PDI. In contrast, photosensitizers with aggregation-induced emission (AIE) characteristics can maintain their ROS generation capacity even in the aggregated state, demonstrating superior therapeutic potential for PDI.[55]

Current AIE photosensitizers effectively address the aggregation-caused quenching (ACQ) effect and demonstrate aggregation-enhanced luminescence and ROS production.[56] Herein, many researchers have focused their attention on tetraphenylethylene (TPE) structures with AIE effects. For instance, Niu's team proposed a tetraphenylethylene-based discrete organoplatinum(II) metallacycle photosensitizer **1**, which employs a TPE structure with AIE characteristics to overcome the ACQ effect of traditional photosensitizers.[57] To further enhance the PDI performance, **1** was assembled with tobacco mosaic virus coat proteins functionalized with a transduction-activating peptide (TAT) to form nanoparticles (**3**) *via* electrostatic interactions (Fig. 1A). The obtained nanoparticles demonstrate excellent ROS generation capacity while maintaining effective bacterial cell membrane penetration capability. This combination of properties synergistically boosts their photodynamic antibacterial efficacy. Fig. 1B clearly reveals that the synergistic effect of membrane embedding ability and ROS generation is the core mechanism for assembly **3** to achieve efficient sterilization. The survival rate of assembly **3** against *E. coli* under light exposure can drop from approximately 55% to nearly 0%. The photosensitizer alone **1** lacks membrane penetration ability, and the bactericidal effect after light exposure is weak. The efficacy of assembly **3′** without TAT modification is significantly reduced (the survival rate only drops from 74% to 63%).

Zhang's group also utilized the TPE structure to construct an antibacterial metalcycle **PtTPEM** (Fig. 1C). They designed a cascaded artificial light capture system (LHS), which significantly enhanced the photodynamic antibacterial efficiency by utilizing collaborative energy transfer.[58] The specific approach is to first coordinate TPE ligands with platinum(II) ions to self-assemble a hexagonal metal ring **PtTPEM** with AIE properties, which serves as an energy donor. Then, the relay molecule sulforhodamine 101 (SR101), which highly overlaps with the PtTPEM emission spectrum, is introduced as the first energy acceptor to further transfer the energy. Finally, the near-infrared photosensitizer chlorophyll e6 (Ce6) is used as the final

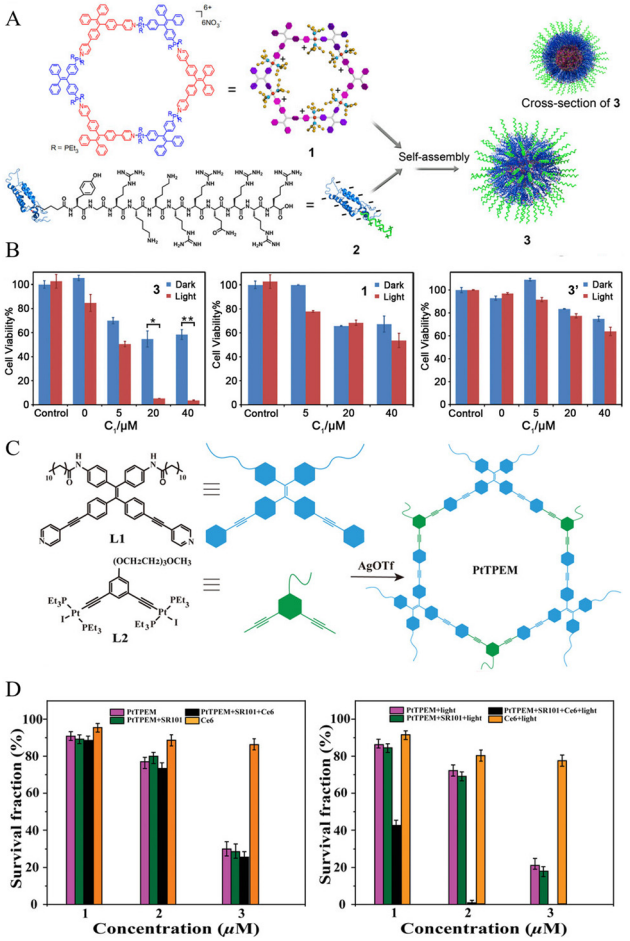

Fig. 1 (A) Schematic illustration of the self-assembly of metallacycle **1**, protein **2** and assembly **3** (B) *E. coli* viability against assembly **3**, metallacycle **1**, and assembly **3′** in the dark and under light irradiation. Reproduced with permission.[57] Copyright 2019, Proceedings of the National Academy of Sciences of the United States of America. (C) Structure of **PtTPEM**. (D) *S. aureus* viability with different concentrations of **PtTPEM** and other different assemblies in the dark or under light conditions. Reproduced with permission.[58] Copyright 2023, Proceedings of the Wiley-VCH.

energy acceptor. Through two-step energy transfer, the light energy is efficiently concentrated, thereby significantly improving the generation efficiency of $^1O_2$. The light-harvesting system (LHS) constructed based on **PtTPEM–SR101–Ce6** exhibited significant light-dependent antibacterial activity. As shown in Fig. 1D, in experiments using *Staphylococcus aureus* as the model organism, the survival rate of bacteria treated with 3 μM **PtTPEM–SR101–Ce6** under white light irradiation dropped to nearly zero, whereas under dark conditions, the survival rate of the similarly treated group remained above 20%. Further intergroup comparisons revealed that the bactericidal effect of the LHS treatment under light was significantly stronger than that of the LHS group kept in darkness or the Ce6-only group, indicating that the system can efficiently achieve light-controlled bacterial inactivation.

Columnar aromatics, with their columnar molecular structure and electron-rich hydrophobic cavities, can efficiently complex charged guest molecules and achieve multifunctionalization through end group modification.[59,60] Therefore, Sun and Stang's group designed a pillar[5]arene-based metallacycle[61] that binds an AIEgen (1-butyl-4-[4-(diphenylamino) styryl]pyridinium) through host–guest interactions (Fig. 2A). The experiment showed that the nanoparticle not only monitors the *in vivo* delivery process of the photosensitizer in real-time but also effectively inhibits bacterial survival through photodynamic effects and significantly accelerates wound healing in mice infected with *S. aureus*. According to the *in vitro* experiments shown in Fig. 2B and C, the supramolecular photosensitizer **1** ⊃ **2** NPs has no obvious toxicity to bacteria in the absence of light, but shows a very strong killing

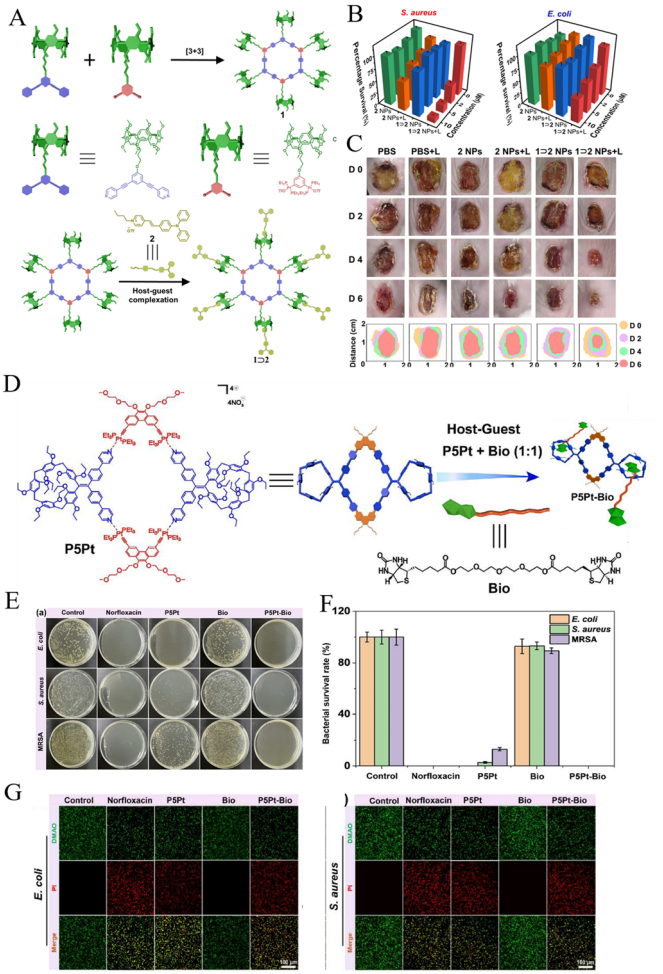

Fig. 2 (A) The structure of metallacycle **1** and the host–guest complexation of **1** ⊃ **2**. (B) Photomicrographs showing *S. aureus* and *E. coli* incubated with **1** ⊃ **2** NPs and **2** NPs for 10 minutes, with or without light irradiation. (C) Photos of mice infected with *S. aureus*. Reproduced with permission.[61] Copyright 2021, Proceedings of the Wiley-VCH. (D) Structure of **P5Pt-Bio**. (E) and (F) Colony-forming unit (CFU) images and bacterial survival rate analysis of Enterobacter, *S. aureus*. (G) Confocal laser scanning microscope (CLSM) image. Reproduced with permission.[62] Copyright 2025, Proceedings of the Springer Nature.

effect on *S. aureus* under 450 nm laser irradiation, and also has a significant inhibitory effect on *E. coli*. *In vivo* experiments further confirm its therapeutic potential. The wounds of the infected mice were significantly healed after treatment with **1** ⊃ **2** NPs. Hu and Yu's group also developed an antibacterial agent using pillararenes—a novel pillar[5]arene-based metallacycle.[62] They utilized the methylene bridging position to construct a supramolecular platinum metallacycle (**P5Pt**), which serves as a host molecule that combines with an ethylene glycol-linked biotin diester linker to form a water-soluble supramolecular nanosystem (**P5Pt-Bio**) (Fig. 2D). This strategy can increase ROS and target membrane destruction, which is a host–guest complex that stimulates reactive bioactivity and biocompatibility. Moreover, the biotin diester coupling linked by ethylene glycol can enhance the water solubility, biocompatibility and antibacterial effect of the metal ring. The study found that **P5Pt-Bio** exhibited excellent antibacterial activity against *E. coli*, *S. aureus* with its MIC for Gram-positive bacteria lower than that of **P5Pt** alone and comparable to norfloxacin, while biocompatibility assays in HaCaT cells revealed enhanced cell viability relative to **P5Pt** (Fig. 2E–G). These findings indicate that the integration of host–guest chemistry with coordination-driven self-assembly opens a new avenue for developing antibacterial platforms that unite real-time imaging and precise therapy, while also laying an important foundation for constructing theranostic antibacterial systems.

Beyond AIE photosensitizers, donor–acceptor–donor (D–A–D)-based photosensitizers have recently demonstrated distinctive advantages in antibacterial applications.[63–65] The D–A–D architecture can effectively modulate the energy level structure through intramolecular charge transfer (ICT), narrowing the energy gap and extending the absorption into the visible or even near-infrared regions.[66,67] Upon coordination with heavy-metal centers, the intersystem crossing (ISC) efficiency and ROS generation can be markedly enhanced, while metal–ligand coordination-driven self-assembly affords excellent water solubility, structural stability, and dual-mode antibacterial activity under both light and dark conditions.[68] A representative example is the Pt(II)$_8$ benzothiadiazole metallosupramolecular tubular cage (**PMB1**) (Fig. 3A) reported by Mukherjee's group whose rigid three-dimensional structure enriches benzothiadiazole photosensitizing units and leverages the heavy-atom effect of platinum to boost $^1O_2$ generation, while the high net positive charge and hydrophobic surface enable strong binding to bacterial membranes, resulting in potent antibacterial activity in both illuminated and dark environments.[69] Under 405 nm excitation, **PMB1** exhibits a significant enhancement in fluorescence intensity (QY = 5.03%) and a 160 nm Stokes shift (Fig. 3B). In antimicrobial tests, **PMB1** demonstrates better antibacterial activity at very low concentrations, regardless of light conditions, while the building units (**L** and **Pt** receptors) show no inhibitory effect against methicillin-resistant *S. aureus* (MRSA) and *Pseudomonas aeruginosa* (PA) under the same conditions (Fig. 3C).

In another study, Sun and Stang's group developed a long-wavelength-emissive Ru(II) metallacycle that extends the D–A–D ligand emission into the second near-infrared (NIR-II, 1000–1700 nm) region,[70] achieving deep-tissue penetration, high spatial resolution, and minimal autofluorescence under 808 nm excitation (Fig. 3D). When they incubated metallacycle **1** with *S. aureus* and *E. coli* to test the interactions with bacteria, metallacycle **1** exhibited a strong near-infrared type II fluorescence signal, and the fluorescence intensity of *S. aureus* was 2.3 times that of *E. coli*, indicating that the absorption efficiency of metallacycle **1** in *S. aureus* was significantly higher than that in *E. coli* (Fig. 3E). In addition, scanning electron microscopy (SEM) characterization revealed that it can cause wrinkles and distortions in the bacterial cell walls, thereby leading to bacterial death (Fig. 3F). Such designs overcome the limitations of traditional photosensitizers, including short excitation wavelengths, poor solubility and ACQ, while offering great potential for multimodal synergistic antibacterial therapy.

In addition to the ACQ effect of photosensitizers, the issue of excessive high-power laser exposure in phototherapy must also be considered.[71–74] Based on this, Sun and Kim's group designed a supramolecular triangle[75] (**Pt1110**) embedded with Pt(II), utilizing an NIR-II emissive boron dipyrromethene

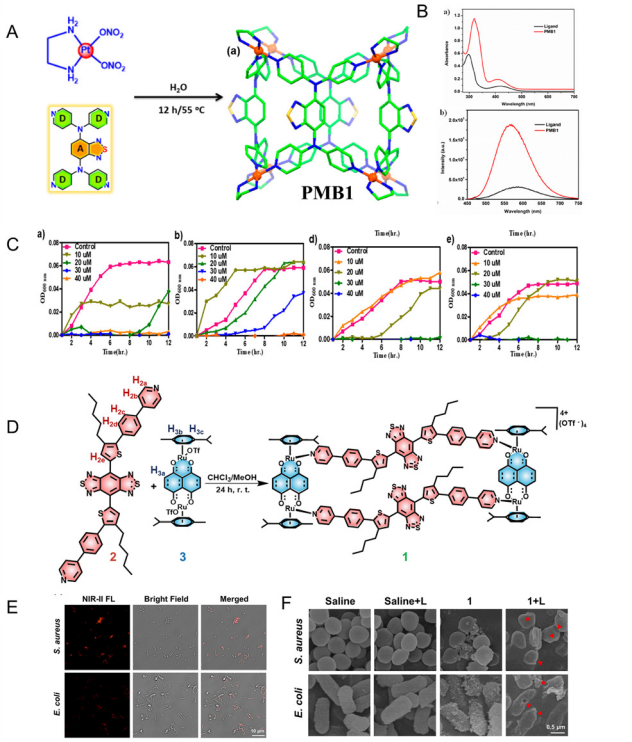

Fig. 3 (A) The structure of **PMB1**. (B) Absorption and emission spectra of PMB1 and L. (C) The growth curve of bacteria in the presence of **PMB1** (ab) and L and Pt (cd): (ac is under light conditions, bd is without irradiation of light). Reproduced with permission.[61] Copyright 2020, Proceedings of the American Chemical Society. (D) Structure of **metallacycle 1**. (E) NIR-II fluorescence images of *S. aureus* and *E. coli* and their fluorescent intensities. (F) Scanning electron microscope res of *S. aureus* and *E. coli* after various treatments. Reproduced with permission.[70] Copyright 2022.

(BODIPY) ligand and a Pt(II) acceptor to achieve coordination-driven [3 + 3] self-assembly(Fig. 4A). The study evaluated the ROS generation ability of **Pt1110**, finding that its oxygen generation yield (Φ_Δ) was 0.28, which is 75% higher than that of ligand **1** (Φ_Δ = 0.16) (Fig. 4B). **Pt1110** enabled precise NIR-II fluorescence imaging and enhanced photoactivated tissue sterilization at a low power density (≤0.72 W cm^{-2}) (Fig. 4D). This phenomenon is likely attributed to the combination of the heavy atom effect and NIR-II excitation. SEM images further showed that **Pt1110** not only strongly adheres to the bacterial surface but also works synergistically with laser irradiation to significantly disrupt the bacterial cell membrane (Fig. 4C). This highlights that structural red-shifting, surface charge modulation, and nanocarrier encapsulation are promising molecular engineering strategies to further advance BODIPY-based supramolecular photosensitizers for antibacterial applications.

The traditional photodynamic therapy (PDT) has made some progress, but its limited tissue penetration remains a challenge.[76,77] In recent years, sonodynamic therapy (SDT) as an emerging antibacterial technology, has gained increasing attention due to its potential to overcome this key limitation of PDT.[78] Sun's team developed a supramolecular sonosensitizer/sonocatalyst (**Ru-A3-TTD**)[79] based on Ru(II) metal rings, achieving a significant breakthrough in the field of sonodynamic antibacterial therapy (Fig. 4E). A series of Ru(II) receptors (Ru-A1, Ru-A2, Ru-A3) were designed in the study using the π expansion strategy, which significantly reduced the molecular orbital energy gap and increased the ROS yield triggered by ultrasound. To verify the effect of **Ru-A3-TTD** in alleviating hypoxia in BME, they assessed the hypoxia levels in MDR *E. coli* infected tissues using immunofluorescence staining of HIF-1α. As shown in Fig. 4F, treatment with **Ru-A3-TTD** resulted in a significant reduction in HIF-1α-positive areas. This suggests that the compound alleviates hypoxia in the BME through its CAT-mimicking activity. **Ru-A3-TTD** effectively addresses three issues in complex BME: alleviating hypoxia to enhance ROS production under ultrasound, disrupting redox balance to protect ROS from GSH consumption, and improving permeability to promote deep ROS generation. This study not only clarified the mechanism of action of the new sonosensitizer by deeply exploring the structure–activity relationship, but also provided an important reference for the treatment and clinical application of biofilm infections.

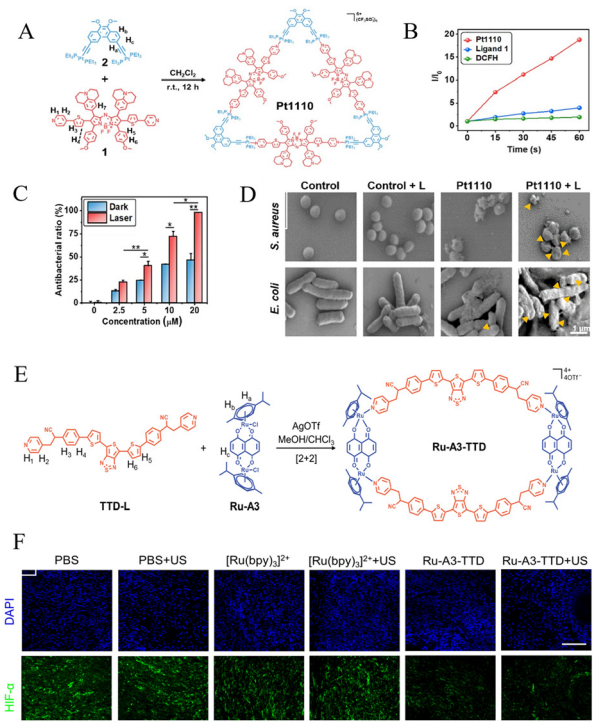

Fig. 4 (A) Synthetic route and structure of **Pt1110**. (B) The ROS generation ability of **Pt1110** and ligand **1**. (C) SEM images of *S. aureus* and *E. coli* treated with **Pt1110**. (D) The antibacterial effect of **Pt1110** on *S. aureus*. Reproduced with permission.[75] Copyright 2022, Proceedings of the Springer Nature. (E) The structure and construction of **Ru-A3-TTD**. (F) Immunofluorescence images of biofilm infections in different treatment groups. Reproduced with permission.[79] Copyright 2024, Proceedings of the Wiley-VCH.

2.2 Physical destruction of bacterial membranes mediated by SCCs

Over the past decade, scientists have achieved notable progress in antimicrobial studies targeting bacterial membranes *via* SCCs.[80,81] Li's group reported a type of SCCs with superior antibacterial properties based on the membrane destruction mechanism.[82] They constructed three generations of nested hexagonal supramolecules (Kandinsky Circles, **G2–G4**) through coordination-driven self-assembly of multidentate terpyridine ligands with Cd(II), with molecular weights reaching 17–38 kDa (Fig. 5A). During the synthesis process of ligands, innovatively modular synthesis is applied to solve the problem of difficult separation of traditional synthetic polydentate ligands. These discrete nested supramolecules tends to form nanoribbon-like structures on the surface of highly oriented pyrolytic graphite (HOPG). Through planar lipid bilayer conductance measurements, they were shown to form transmembrane channels (conductance 15–26 pS) (Fig. 5B), while fluorescence microscopy and TEM ultrathin sections revealed membrane insertion leading to cytoplasmic leakage. **G2–G4** exhibit potent antibacterial activity against Gram-positive MRSA with negligible toxicity to eukaryotic cells, achieving bactericidal effects by disrupting cell membranes and inducing ion leakage (Fig. 5C and D). This nested multivalent design with large rigid structures significantly enhanced membrane interaction, providing a template for developing highly specific membrane-disrupting agent.

In 2019, the team made further improvements to the synthetic method.[83] They developed a multicomponent one-pot synthesis/self-assembly strategy by combining irreversible condensation of pyrylium salts with primary amines and tpy-Zn coordination, successfully constructing complex two-dimensional spiderweb-like molecules (**SW-1** and **SW-2**) (Fig. 5E). This method enables direct precipitation purification of the

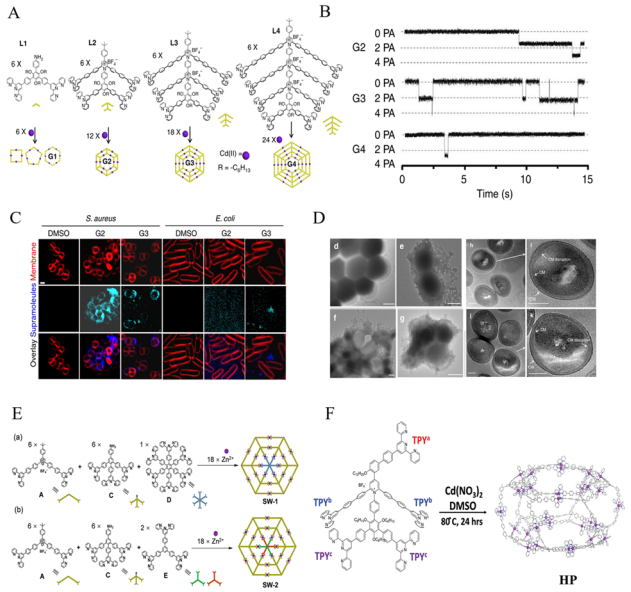

Fig. 5 (A) Self-assembly and the structure of **G1**–**G4**. (B) Conductance measurement of **G2**–**G4** in planar lipid bilayers. Reproduced with permission.[82] (C) **G2**–**G3** deconvolution fluorescence microscope images. (D) TEM images of **G2**–**G4**. (E) Structure of **SW-1** and **SW-2**. Reproduced with permission.[83] Copyright 2019, Proceedings of the American Chemical Society. (F) Structure of **HP**. Reproduced with permission.[84] Copyright 2021, Proceedings of the Royal Society of Chemistry.

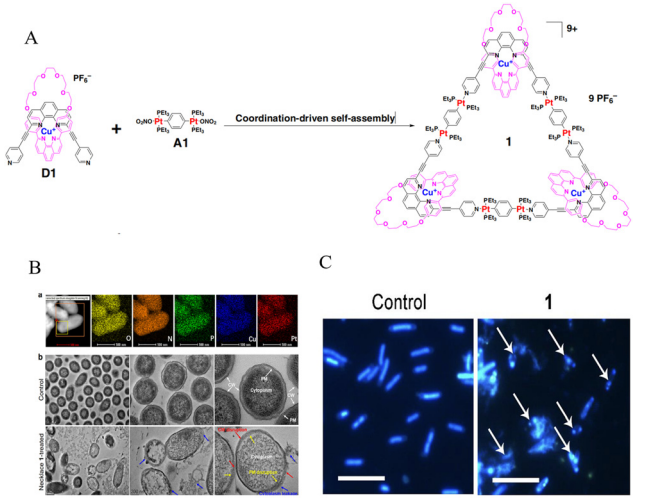

Fig. 6 (A) Self-assembly and the structure of **1**. (B) The energy dispersion spectrum of element co-localization. (C) TEM images of **1**. Reproduced with permission.[85] Copyright 2020, Proceedings of Springer Nature.

target product without intermediate isolation. The work provides a new methodology for high-throughput synthesis of bioactive supramolecules, highlighting how orthogonal self-assembly can efficiently generate complex functional architectures for biomedical applications.

In 2021, Nieh and Li's group constructed a novel nanocomplex, **HP-B**, which is formed by encapsulating the hydrophobic antibacterial supramolecule **HP** within niform-sized discoidal bicelles (Fig. 5F). This nanocomposite significantly enhances the water solubility and biocompatibility of **HP**.[84] It adopts a hexagonal parallel (non-stacked) configuration along the high-curvature edges of bicelles, effectively minimizing π–π interactions and significantly enhancing fluorescence emission intensity. In terms of the antibacterial mechanism, **HP** itself exhibits direct antibacterial activity against Gram-positive bacteria. Meanwhile, the bicelles enhance the stability of **HP** in biological environments, thereby facilitating the delivery of more **HP** to its target sites.

In 2020, Yang's team synthesized the first heterometallic triangular necklace structure containing both Cu and Pt metals through a highly efficient metal-coordination-driven "threading-followed-by-ring-closing" strategy.[85] This architecture features a precise interlocked assembly comprising a large [3 + 3] Pt(II)–N cationic metallacycle and three polyether phenanthroline macrocycles(**1**) (Fig. 6A). To explore its antibacterial mechanism, researchers first found through energy dispersive spectroscopy that copper and platinum elements were significantly enriched on the cell surface and co-localized with cellular components such as oxygen, nitrogen, and phosphorus, preliminarily confirming that the necklace structure can directly contact the cell surface (Fig. 6B). Further observation by transmission electron microscopy revealed that the bacterial cells treated with this heterogeneous metal necklace generally suffered from severe damage to the cell wall and plasma membrane, resulting in cytoplasmic leakage (Fig. 6C), demonstrating a strong membrane destruction effect. The heterometallic Cu(I)/Pt(II) system significantly enhances antibacterial efficacy by synergistically strengthening bacterial binding and disruption through electrostatic interactions, while concurrently inducing DNA breakage. This work represents the first reported heterometallic molecular necklace and establishes a new paradigm for designing mechanically interlocked molecules with enhanced biological functions.

Chen and Yang's group developed a class of discrete saccharide-functionalized amphiphilic metallacycles—namely **[2 + 2]-Gal**, **[3 + 3]-Gal**, and **[6 + 6]-Gal**—*via* coordination-driven self-assembly[86] (Fig. 7A). As shown in Fig. 7B, these structures demonstrated size and carbohydrate-dependent hierarchical self-assembly in aqueous environments, leading to the formation of diverse nanostructures including nanoparticles, vesicles, and micron-scale vesicles. Dissipative particle dynamics (DPD) simulations further illuminated the self-assembly mechanism, highlighting a delicate interplay between hydrophobic/π–π stacking within the metallacyclic core and inter-galactoside carbohydrate-carbohydrate interactions (CCIs), which was particularly distinctive in the case of **[6 + 6]-Gal**. When evaluated for bioactivity, these glyco-metallacycles exhibited pronounced antibacterial and anti-biofilm effects against *S. aureus*. The **[6 + 6]-Gal** micron-sized vesicles stood out, showing potent biofilm inhibition at concentrations as low as 12.5 μM, markedly surpassing the performance of the non-glycosylated analogue **[3 + 3]-EG5**. The anti-biofilm

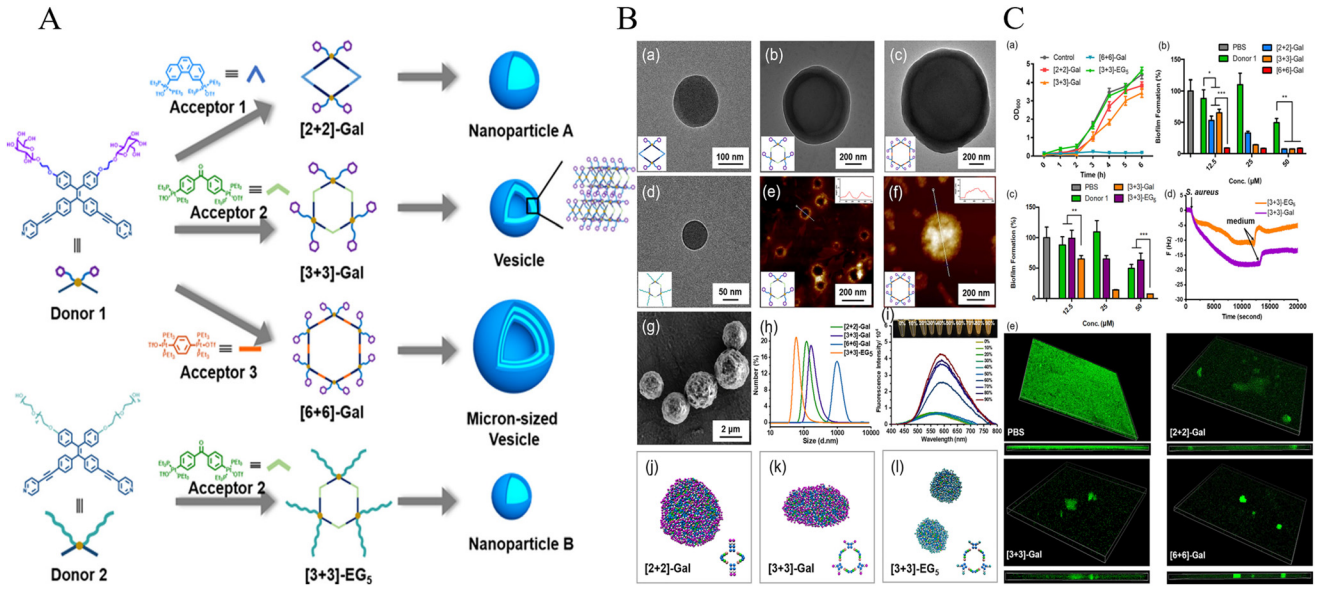

Fig. 7 (A) A graphical depiction of the formation and hierarchical self-assembly structures of amphiphilic metallacycles. (B) The representation diagram of **[2 + 2]-Gal**, **[3 + 3]-Gal**, **[6 + 6]-Gal**, **[3 + 3]-EG$_5$**. (C) The antibacterial activity of metallacycle assemblies. Reproduced with permission.[86] Copyright 2020, Proceedings of the American Chemical Society.

efficacy was visually substantiated through confocal laser scanning microscopy (CLSM), where treated samples showed nearly complete absence of biofilm formation (Fig. 7C). Mechanistic studies revealed a dual mode of action: initial bacterial attachment was facilitated by electrostatic interactions between the positively charged metallacycles and negatively charged cell surfaces, while quartz crystal microbalance (QCM) assays underscored the critical contribution of specific galactoside-mediated "sweet talking" interactions in achieving strong bacterial binding and biofilm inhibition—a mechanism absent in EG5-modified controls. This work successfully integrates precision supramolecular assembly with carbohydrate bioactivity, offering a novel and efficient strategy to combat biofilm-associated infections through rational metallacycle design.

The above research content demonstrates how precisely controlling molecular geometry, metal composition, and self-assembly pathways can generate complex materials with enhanced biological activity, providing valuable insights for the development of next-generation antibacterial agents that operate through physical membrane destruction mechanisms.

2.3 The antibacterial mechanisms of metal supramolecular networks

Supramolecular network materials have shown great potential in the antibacterial field due to their unique structures and functions. By introducing metal complexes as cross-linking points or functional units, researchers have successfully constructed a series of metal supramolecular networks with high antibacterial performance.[87–89] In 2020, Zhang's group prepared a supramolecular network based on poly(*N*-isopropylacrylamide) (**PNIPAAM**),[90] cross-linked by a fluorescent hexagonal platinum(II) metal ring (Fig. 8A). This network can not only be used for bacterial imaging but also effectively kill bacteria. The antibacterial mechanism mainly relies on the ability of the platinum(II) metal ring to disrupt the bacterial cell wall and membrane structure, while the water solubility and bioavailability of **PNIPAAM** further enhance the antibacterial performance of the network (Fig. 8B). Table 1 in Fig. 8 shows that the network with the highest cross-linking density (**5a**) exhibited the strongest antibacterial activity against *E. coli* and *S. aureus*, with minimum inhibitory concentrations (MICs) of 25 μg mL^{-1} and 12.5 μg mL^{-1}, respectively. As shown in the morphological images of *E. coli* and *S. aureus*, the bacterial cell walls were totally damaged after incubation with supramolecular networks **5a** (Fig. 8C). Building on this research, subsequent studies further explored the applications of metal supramolecular networks in the antibacterial field. In 2024, they used a platinum(II)/copper(I) heterometal[2]rotaxane as the cross-linking unit and cross-linked it with polyethylene glycol (PEG) *via* click reaction to construct a novel supramolecular network (**P1**–**P3**) (Fig. 8D). This network exhibited broad-spectrum and highly efficient antibacterial activity against various bacteria, including methicillin-resistant *S. aureus* (MRSA), due to the synergistic antibacterial effects of platinum (II) and copper(I) ions. As shown in Fig. 8E, the network **P1** had antibacterial rates of 99.7% and 98.4% against *E. coli* and *S. aureus* respectively, and could completely kill MRSA at a concentration of 40 μM. Moreover, scanning electron microscope (SEM) images showed that supramolecular network **P1** caused the most severe damage to the bacterial cell wall, consistent with the antibacterial activity results.[91]

In 2025, this team prepared a free aestanding supramolecular network (**6a**–**6c**)[92] by photoinduced copolymerization, cross-linking a platinum(II) metal cage (**4**) with butyl methacry-

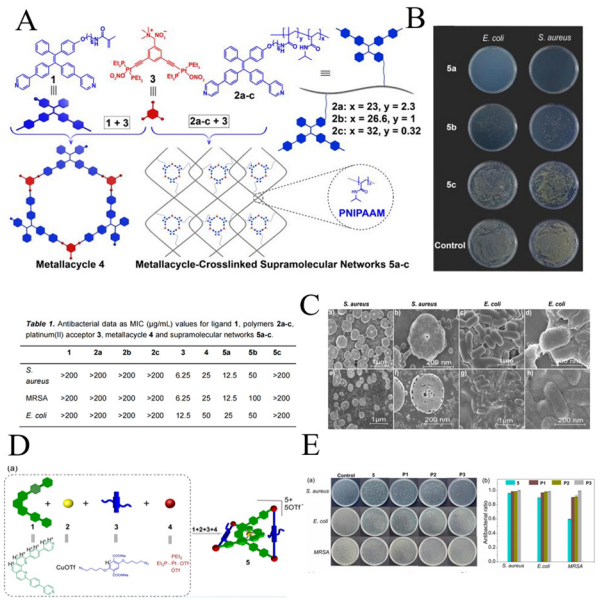

Table 1. Antibacterial data as MIC (μg/mL) values for ligand 1, polymers 2a-c, platinum(II) acceptor 3, metallacycle 4 and supramolecular networks 5a-c.

	1	2a	2b	2c	3	4	5a	5b	5c
S. aureus	>200	>200	>200	>200	6.25	25	12.5	50	>200
MRSA	>200	>200	>200	>200	6.25	25	12.5	100	>200
E. coli	>200	>200	>200	>200	12.5	50	25	50	>200

Fig. 8 (A) Structure of **PNIPAAM**. (B) The effect of supramolecular networks **5a–c** on the colonies of *E. coli* and *S. aureus*. (C) SEM images of **5a**. Reproduced with permission.[90] Copyright 2022, Proceedings of Wiley-VCH. (D) Structure of heterometallic[2]catenane-crosslinkedsupramolecular networks **P1–P3**. (E) The antibacterial effects images of **5** and **P1–P3** against *S. aureus*, *E. coli* and MRSA. Reproduced with permission.[91] Copyright 2024, Proceedings of Wiley-VCH.

late (**5**) (Fig. 9A). This network, due to the photosensitizing ability of the metal cage, could efficiently generate $^1O_2$ under light irradiation, thereby degrading and killing organic pollutants and bacteria. Experimental results indicated that network **6c** achieved the highest methyl orange degradation efficiency, reaching 8.016% after 30 minutes of light irradiation. It also exhibited strong antibacterial activity against *E. coli* and *S. aureus*, with minimum bactericidal concentrations (MBCs) of 0.004 mg and 0.01 mg, respectively (Fig. 9B). Moreover, the network demonstrated good recyclability and reusability, highlighting its strong potential for practical water treatment applications.[93]

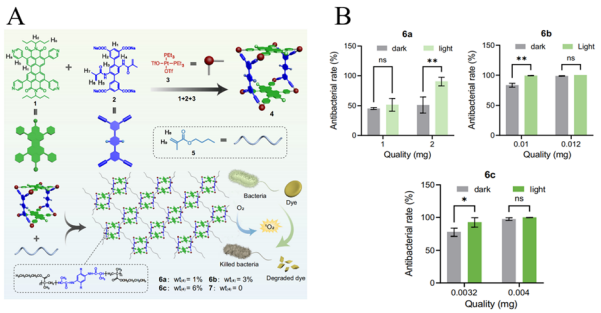

Fig. 9 (A) Synthetic routes and structure of metallacage-crosslinked supramolecular networks (**6a–6c**). (B) The antibacterial activity of supramolecular networks **6a**, **6b** and **6c** against *S. aureus*. Reproduced with permission.[92] Copyright 2022, Proceedings of the National Academy of Sciences of the United States of America.

These researches have demonstrated the great potential of metal supramolecular network materials in the antibacterial field. From the initial combination of fluorescent imaging and antibacterial functions, to the exploration of synergistic antibacterial effects and photocatalytic antibacterial mechanisms, these studies have not only deepened the understanding of the antibacterial properties of metal supramolecular networks but also provided important references and ideas for the development of new antibacterial materials.

3. Conclusions and perspective

This article briefly introduces the latest progress in antibacterial strategies based on reactive oxygen-mediated and physical–mechanical destruction mechanisms, and further discusses how these mechanisms inform the molecular engineering of SCCs for antibacterial applications.

In ROS-mediated systems, the coordination self-assembly of photosensitizers or sonosensitizers with metal centers enables controllable and efficient ROS production for PDT and SDT, thereby enhancing antibacterial efficacy.[94,95] In parallel, physicomechanical mechanisms rely on the membrane-penetrating ability and electrostatic interactions of SCCs to induce membrane rupture and ion leakage, effectively leading to bacterial death.[96] Moreover, metal-ion-crosslinked supramolecular networks have demonstrated synergistic antibacterial activity by reinforcing structural stability and amplifying membrane disruption.[97] Although these two mechanisms have achieved certain results, there are still some problems that need to be solved urgently at present:

(1) At present, heavy metal elements such as Pt and Ru used in SCCs pose potential toxicity risks.[98] Although previous studies have attempted to enhance its biocompatibility through host–guest chemical modifications, the long-term biosafety issue has not been fundamentally resolved. Future research could shift towards molecular engineering strategies, such as replacing heavy metals with light metal elements, thereby systematically reducing the toxicity of these materials.

(2) Second, current antibacterial agents, especially photosensitizer-based PDT, have shown great potential in the treatment of local infections due to their non-invasive nature and low likelihood of inducing drug resistance.[99] However, their therapeutic effect is limited by the limited tissue penetration ability of visible light (usually <0.5 cm), making it difficult to effectively act on deep tissue infections. In contrast, SDT takes advantage of the stronger tissue penetration ability of ultrasound (<10 cm) and shows greater potential in the treatment of deep infections.[100–102] However, at present, there are relatively few studies on the application of ultrasound sensitizers in antibacterial diagnosis and treatment. Therefore, it is very necessary to develop new types of sonosensitizers to promote the in-depth development of antibacterial sonodynamic therapy.

(3) In addition, the targeting ability of SCCs still needs to be improved,[103] although SCCs possess excellent structural tunability and exhibit multiple antibacterial mechanisms,

their targeting capability remains limited, making it difficult to achieve precise recognition and action toward specific pathogens or infection sites.[104] Most SCCs rely on positively charged metal centers or cationic ligands to interact non-specifically with bacterial membranes through electrostatic and hydrophobic interactions. While such interactions confer broad-spectrum antibacterial effects, they lack selectivity and may induce cytotoxicity toward host cells.[105,106] Future studies could focus on refining ligand structures by incorporating bacteria-specific recognition motifs—such as carbohydrate receptor ligands, antimicrobial peptide sequences, or siderophore analogs—and on optimizing the coordination geometry between metal centers and ligands to enhance specific molecular interactions with bacterial membranes, thereby achieving more efficient and selective antibacterial targeting.

Currently, the key challenges in the clinical translation of supramolecular coordination complexes (SCCs) mainly include insufficient *in vivo* stability and limited controllability over their metabolic behavior.[107] In complex physiological environments, SCCs are prone to nonspecific distribution, making it difficult to maintain adequate effective drug concentrations at target sites. Additionally, a systematic safety evaluation framework for their long-term use remains to be established.

To address these challenges, one important direction for SCCs is to develop intelligent drug delivery systems capable of responding to the local microenvironment. Among these, one of the most promising pathways for clinical translation involves the development of surface functional coatings to combat biofilm-related infections.[108] For example, in localized infection models such as chronic wound infections or implant-associated infections, SCCs can be flexibly designed into hydrogel, nanofiber, or functional coating materials.[109] Such formulations can sense specific signals in the infected microenvironment (*e.g.*, pH, enzymes, or redox states), enabling controlled release and targeted accumulation of antibacterial components at the lesion site.[110] This not only significantly enhances treatment efficacy but also helps reduce systemic toxic side effects, while providing a more controllable drug delivery basis for long-term safety performance evaluation.

Author contributions

Qiao Song: writing – original draft; Junhua Zhang: writing; Lulu Yan: writing – editing; Zhipeng Zhang: review; Junrong Li: drawing figures; Yao Sun: writing – review & editing.

Conflicts of interest

There are no conflicts to declare.

Data availability

No primary research results, software or code have been included and no new data were generated or analysed as part of this review.

Acknowledgements

We thank the National Natural Science Foundation of China (22374055, 22022404, 22474047, and 22204055), the National Natural Science Foundation of Hubei Province (2022CFA033, 2025AFB947), the Fundamental Research Funds for the Central Universities (2662025SYPY005), supported by the Open Project Program of Wuhan National Laboratory for Optoelectronics NO. 2024WNLIKF001.

References

1 A. Yarahmadi, H. Najafiyan, M. H. Yousefi, E. Khosravi, E. Shabani, H. Afkhami and S. S. Aghaei, *Front. Cell. Infect. Microbiol.*, 2025, **15**, e10355.
2 E. Cordisco and D. O. Serra, *Trends Microbiol.*, 2025, **33**, 459–471.
3 C. J. Pedersen, *Angew. Chem., Int. Ed. Engl.*, 1988, **27**, 1021–1027.
4 G. Wu, Z. Xu, Y. Yu, M. Zhang, S. Wang, S. Duan and X. Liu, *Front. Pharmacol.*, 2024, **15**, 1513850.
5 S. B. Levy and B. Marshall, *Nat. Med.*, 2004, **10**, S122–S129.
6 Himanshu, R. Mukherjee, J. Vidic, E. Leal, A. C. da Costa, C. R. Prudencio, V. S. Raj, C.-M. Chang and R. P. Pandey, *Biomolecules*, 2023, **13**, 1182.
7 J. G. Hardy, M. Palma, S. J. Wind and M. J. Biggs, *Adv. Mater.*, 2016, **28**, 5717–5724.
8 S. Nolivos, J. Cayron, A. Dedieu, A. Page, F. Delolme and C. Lesterlin, *Science*, 2019, **364**, 778–782.
9 B. Jia, A. Raphenya, B. Alcock, N. Waglechner, P. Guo, K. Tsang, B. Lago, B. Dave, S. Pereira, A. Sharma, S. Doshi, M. Courtot, R. Lo, L. Williams, J. Frye, T. Elsayegh, D. Sardar, E. Westman, A. Pawlowski, T. Johnson, F. L. Brinkman, G. Wright and A. McArthur, *Nucleic Acids Res.*, 2017, **45**, D566–D573.
10 H. C. Flemming, J. Wingender, U. Szewzyk, P. Steinberg, S. A. Rice and S. Kjelleberg, *Nat. Rev. Microbiol.*, 2016, **14**, 563–575.
11 L. Dieltjens, K. Appermans, M. Lissens, B. Lories, W. Kim, E. V. Van der Eycken, K. R. Foster and H. P. Steenackers, *Nat. Commun.*, 2020, **11**, 107.
12 K. K. Sakimoto, C. Liu, J. Lim and P. D. Yang, *Nano Lett.*, 2014, **14**, 5471–5476.
13 B. Tse Sum Bui, T. Auroy and K. Haupt, *Angew. Chem., Int. Ed.*, 2022, **61**, e202106493.
14 G. D. Wright, *Nat. Rev. Microbiol.*, 2007, **5**, 175–186.
15 D. Han, X. Liu and S. Wu, *Chem. Soc. Rev.*, 2022, **51**, 7138–7169.
16 R. Li, T. Chen and X. Pan, *ACS Nano*, 2021, **15**, 3808–3848.
17 X. Liu, D. Huang, C. Lai, G. Zeng, L. Qin, H. Wang, H. Yi, B. Li, S. Liu, M. Zhang, R. Deng, Y. Fu, L. Li, W. Xue and S. Chen, *Chem. Soc. Rev.*, 2019, **48**, 5266–5302.
18 C. Gao, L. Fu, J. Wang, Y. Chu, L. Gao, H. Qiu and J. Chen, *Chem. Biomed. Imaging*, 2025, **3**, 837–848.

19 B. Sun, Z. Ye, M. Zhang, Q. Song, X. Chu, S. Gao, Q. Zhang, C. Jiang, N. Zhou, C. Yao and J. Shen, *ACS Appl. Mater. Interfaces*, 2021, **13**, 42396–42410.
20 D. Yan, Y. Huang, J. Zhang, Q. Wu, G. Song, J. Ji, Q. Jin, D. Wang and B. Tang, *J. Am. Chem. Soc.*, 2023, **145**, 25705–25715.
21 X. Li, H. Bai, Y. Yang, J. Yoon, S. Wang and X. Zhang, *Adv. Mater.*, 2019, **31**, 1805092.
22 L. Gao, H. Wang, B. Zheng and F. Huang, *Giant*, 2021, **7**, 100066.
23 F. Gao, T. Shao, Y. Yu, Y. Xiong and L. Yang, *Nat. Commun.*, 2021, **12**, 745.
24 D. Yan, Y. Huang, J. Zhang, Q. Wu, G. Song, J. Ji, Q. Jin, D. Wang and B. Tang, *J. Am. Chem. Soc.*, 2023, **145**, 25705–25715.
25 J. Xie, C. Liang, S. Luo, Z. Pan, Y. Lai, J. He, H. Chen, Q. Ren, H. Huang, Q. Zhang and P. Zhang, *ACS Appl. Mater. Interfaces*, 2021, **13**, 27934–27944.
26 C. R. Johnson, M. N. Tran, L. M. Michelitsch, S. Abraham, J. L. Hu, K. A. Gray and E. M. Hartmann, *J. Hazard. Mater.*, 2020, **396**, 122445.
27 J. Wang, L. Zhuo, W. Liao, X. Yang, Z. Tang, Y. Chen, S. Luo and Z. Zhou, *ACS Appl. Mater. Interfaces*, 2017, **9**, 7964–7971.
28 S. Sun, X. Liu, X. Meng, Z. Yang, X. Zhang and H. Dong, *ACS Nano.*, 2025, **19**, 15109–15119.
29 A. Peter, J. Joseb, S. G. Bhat and K. Abhitha, *Results Eng.*, 2024, **24**, 102925.
30 J. D. Richardson and R. C. Van Lehn, *J. Phys. Chem. B*, 2025, **129**, 9983–9997.
31 P. Zhu, Y. Chen and J. Shi, *ACS Nano*, 2018, **12**, 3780–3795.
32 S. E. Rossiter, M. H. Fletcher and W. M. Wuest, *Chem. Rev.*, 2017, **117**, 12415–12474.
33 C. C. Mayorga-Martinez, L. Zhang and M. Pumera, *Chem. Soc. Rev.*, 2024, **53**, 2284–2299.
34 L. Li, Y. Xie, J. Wang, Q. Sun, M. Gao and C. Li, *Acta Biomater.*, 2024, **183**, 221–234.
35 Y. Qin, X. Chen, Y. Gui, H. Wang, B. Tang and D. Wang, *J. Am. Chem. Soc.*, 2022, **144**, 12825–12833.
36 H. Sepehrpour, W. X. Fu, Y. Sun and P. J. Stang, *J. Am. Chem. Soc.*, 2019, **141**, 14005–14020.
37 Z. Zhang, H. Ye, F. Cai and Y. Sun, *Dalton Trans.*, 2023, **52**, 15193–15202.
38 J. Li, Y. Liu, Y. Xu, L. Li, Y. Sun and W. Huang, *Coord. Chem. Rev.*, 2020, **415**, 213318.
39 Y. Pang, C. Li, H. Deng and Y. Sun, *Dalton Trans.*, 2022, **51**, 16428–16438.
40 F. Zhao, Y. Xu, M. Lu, L. Tu, C. Li, Y. Dou, J. Li, X. Li and Y. Sun, *J. Nanobiotechnol.*, 2025, **23**, 430.
41 F. Zhao, Y. Pang, Q. Song, J. Zhang, Y. Li, S. Qiu and Y. Sun, *Chin. J. Chem.*, 2025, **43**, 2810–2824.
42 B. B. Ismail, Q. He, D. Liu and M. Guo, *Crit. Rev. Food Sci. Nutr.*, 2025, **18**, 1–26.
43 J. Liu, D. Wu, N. Zhu, Y. Wu and G. Li, *Trends Food Sci. Technol.*, 2021, **109**, 413–434.
44 C. Li, L. Tu, J. Yang, C. Liu, Y. Xu, J. Li, W. Tuo, B. Olenyuk, Y. Sun, P. J. Stang and Y. Sun, *Chem. Sci.*, 2023, **14**, 2901–2909.
45 H. Jia, T. Shi, T. He, Y. Li and S. Yin, *Dalton Trans.*, 2023, **52**, 4296–4302.
46 Y. Sun, F. Ding, Z. Zhou, C. Li, M. Pu, Y. Xu, Y. Zhan, X. Lu, H. Li, G. Yang, Y. Sun and P. J. Stang, *Proc. Natl. Acad. Sci. U. S. A.*, 2019, **116**, 1968–1973.
47 F. Ding, Z. Chen, W. Kim, A. Sharma, C. Li, Q. Y. Ouyang, H. Zhu, G. Yang, Y. Sun and J. S. Kim, *Chem. Sci.*, 2019, **10**, 7023–7028.
48 Q. Li, H. Ye, F. Zhao, Y. Li, Z. Zhang, Q. Yan and Y. Sun, *Dalton Trans.*, 2024, **53**, 3434–3444.
49 Y. Qin, X. H. Chen, Y. X. Gui, H. Wang, B. Z. Tang and D. Wang, *J. Am. Chem. Soc.*, 2022, **144**, 12825–12833.
50 L. Yang, S. Huang, J. Chen, P. Xiao, J. Sun, Y. Jiang and H. Sun, *Chem. Biomed. Imaging*, 2025, DOI: 10.1021/cbmi.5c00169.
51 Y. Zhang, Q. Zhang, F. Wang, M. Li, X. Shi and J. Li, *Nano Lett.*, 2023, **23**, 7699–7708.
52 S. Saha, R. Majumdar, A. Hussain, R. R. Dighe and A. R. Chakravarty, *Philos. Trans. R. Soc., A*, 2013, **371**, 20120190.
53 H. Shi, W. Sun, Q. Wang, G. Gu, W. Si, W. Huang, Q. Zhang and X. Dong, *ChemPlusChem*, 2016, **81**, 515–520.
54 N. Niu, H. Zhou, N. Liu, H. Jiang, Z. Hu and C. Yu, *Chem. Commun.*, 2020, **56**, 1608–1608.
55 Z. Gong and Z. Dai, *Adv. Sci.*, 2021, **8**, 2002178.
56 W. Wen, J. Li, W. Shang, Z. Zhuang, X. Deng, X. Yan, D. Xie, C. Cui, Z. Zhao, B. Tang and H. Su, *Mater. Today Bio*, 2025, **32**, 101828.
57 S. Gao, X. Yan, G. Xie, M. Zhu, X. Ju, P. J. Stang, Y. Tian and Z. W. Niu, *Proc. Natl. Acad. Sci. U. S. A.*, 2019, **116**, 23437–23443.
58 M. Chen, Z. Lu, M. Li, B. Jiang, S. Liu, Y. Li, B. Zhang, X. Li, T. Yi and D. Zhang, *Adv. Healthcare Mater.*, 2023, **12**, 2300377.
59 M. Ball, Y. Zhong, Y. Wu, C. Schenck, F. Ng, M. Steigerwald, S. X. Xiao and C. Nuckolls, *Acc. Chem. Res.*, 2015, **48**, 267–276.
60 S. K. Pathak, B. Pradhan, R. K. Gupta, M. Gupta, S. K. Pal and A. S. Achalkumar, *J. Mater. Chem. C*, 2016, **4**, 6117–6130.
61 Y. Xu, W. Tuo, L. Yang, Y. Sun, C. Li, X. Chen, W. Yang, G. Yang, P. Stang and Y. Sun, *Angew. Chem., Int. Ed.*, 2022, **61**, e202110048.
62 P. Jeyakkumar, K. H. Du, R. B. Zhang, X. Q. Tian, Q. Liu, J. M. Jiao, H. Jiang, X. J. Yu and X. Y. Hu, *Sci. China: Chem.*, 2025, **17**, 1–7.
63 X. Yan, P. Wei, Y. Liu, M. Wang, C. Chen, J. Zhao, G. Li, M. Saha, Z. Zhou, Z. An, X. Li and P. Stang, *J. Am. Chem. Soc.*, 2019, **141**, 9673–9679.
64 S. Kumar, M. Kumar, H. Bhambri, S. K. Mandal and V. Bhalla, *ACS Appl. Mater. Interfaces*, 2024, **16**, 67683–67696.
65 Z. Zhang, G. Gou, J. Wan, H. Li, M. Wang and L. Li, *J. Org. Chem.*, 2022, **87**, 2470–2479.

66 Y. Li, P. Han, X. Zhang, J. Zhou, X. Qiao, D. Yang, A. Qin, B. Tang, J. Peng and D. Ma, *J. Mater. Chem. C*, 2023, **11**, 3284–3291.
67 X. Mei, S. Yao, L. Xu, Y. Shi, H. Yang, S. Zhou, J. Zhang, M. Yan, J. Yu and Y. Zhang, *Sen. Actuators, B*, 2025, **431**, 137432.
68 A. Morimoto, K. Shimizu, N. Suzuki, S. Yagi, K. Sueyoshi, T. Endo and H. Hisamoto, *Analyst*, 2024, **149**, 1939–1946.
69 S. Bhattacharyya, M. Venkateswarulu, J. Sahoo, E. Zangrando, M. De and P. S. Mukherjee, *Inorg. Chem.*, 2020, **59**, 12690–12699.
70 Y. Xu, C. Li, X. Ma, W. Tuo, L. Tu, X. Li, Y. Sun, P. J. Stang and Y. Sun, *Proc. Natl. Acad. Sci. U. S. A.*, 2022, **119**, e2209904119.
71 J. Zhou, G. Yu and F. Huang, *Chem. Soc. Rev.*, 2017, **46**, 7021–7053.
72 Y. Zhang, Q. Wang, Z. Zhu, W. Zhao, C. Yan, Z. Liu, M. Liu, X. Zhao, H. Tian and W. Zhu, *CCS Chem.*, 2022, **4**, 1619–1632.
73 B. Ran, Z. Wang, W. Cai, L. Ran, W. Xia, W. Liu and X. Peng, *J. Am. Chem. Soc.*, 2021, **143**, 17891–17909.
74 Y. Sun, C. Chen, J. Liu and P. J. Stang, *Chem. Soc. Rev.*, 2020, **49**, 3889–3919.
75 Y. Xu, C. Li, J. An, X. Ma, J. Yang, L. Luo, Y. Deng, J. Kim and Y. Sun, *Sci. China: Chem.*, 2023, **66**, 155–163.
76 P. Jeyakkumar, P. Jeyakkumar, Y. Liang, M. Guo, S. Lu, D. Xu, X. Li, B. Guo, G. He, D. Chu and M. Zhang, *Angew. Chem., Int. Ed.*, 2020, **59**, 15199–15203.
77 J. Wang, S. Gao, X. Wang, H. Zhang, X. Ren, J. Liu and F. Bai, *Nano Res.*, 2022, **15**, 2347–2354.
78 J. Zhu, L. Xu, Y. Ren, Y. Zhang, X. Liu, G. Yin, B. Sun, X. Cao, Z. Chen, X. Zhao, H. Tang, J. Chen, X. Li and H. Yang, *Nat. Commun.*, 2019, **10**, 2369–2416.
79 Y. Xu, Y. Pang, L. Luo, A. Sharma, J. Yang, C. Li, S. Liu, J. Zhan and Y. Sun, *Angew. Chem., Int. Ed.*, 2024, **63**, e202319966.
80 A. N. Singh, J. B. Nice, M. S. Wu, A. C. Brown and N. J. Wittenberg, *Chem. Biomed. Imaging*, 2024, **2**, 352–361.
81 J. H. Kim, X. W. Wang, C. L. Zhang, S. A. Yoon, J. Shin, A. Sharma, M. H. Lee, L. Cheng, J. S. Wu and J. S. Kim, *Chem. Soc. Rev.*, 2020, **49**, 3244–3261.
82 H. Wang, X. Qian, K. Wang, M. Su, W. Haoyang, X. Jiang, R. Brzozowski, M. Wang, X. Gao, Y. Li, B. Xu, P. Eswara, X. Hao, W. Gong, J. Hou, J. Cai and X. Li, *Nat. Commun.*, 2018, **9**, 1815.
83 H. Wang, Y. Li, H. Yu, B. Song, S. Lu, X. Hao, Y. Zhang, M. Wang, S. W. Hla and X. Li, *J. Am. Chem. Soc.*, 2019, **141**, 13187–13195.
84 C. Liu, H. Wang, L. Yang, Y. Liu, X. Li and M. P. Nieh, *Nanoscale*, 2021, **13**, 14973–14979.
85 G. Wu, X. Shi, H. Phan, H. Qu, Y. Hu, G. Yin, X. Zhao, X. Li, L. Xu, Q. Yu and H. Yang, *Nat. Commun.*, 2020, **11**, 3178.
86 G. Tao, T. Ji, N. Wang, G. Yang, X. Lei, W. Zheng, R. Liu, X. Xu, L. Yang, G. Yin, X. Liao, X. Li, H. Ding, X. Ding, J. Xu, H. Yang and G. Chen, *ACS Macro Lett.*, 2020, **9**, 61–69.
87 X. Yan, F. Wang, B. Zheng and F. Huang, *Chem. Soc. Rev.*, 2012, **41**, 6042–6065.
88 S. Begum, Z. Hassan, S. Bräse, C. Wöll and M. Tsotsalas, *Acc. Chem. Res.*, 2019, **52**, 1598–1610.
89 X. Ma and H. Tian, *Acc. Chem. Res.*, 2014, **47**, 1971–1981.
90 G. Takayama and T. Kondo, *Carbohydr. Polym.*, 2023, **321**, 121311.
91 R. Li, H. Zhang, Y. Hou, L. Gao, D. Chu and M. Zhang, *Nat. Commun.*, 2025, **16**, 2733.
92 Q. Feng, R. Ding and M. Zhang, *Chem. – Eur. J.*, 2025, **31**, e202403595.
93 L. He, Y. Jiang, J. Wei, Z. Zhang, T. Hong, Z. Ren, J. Huang, F. H. Huang, P. Stang and S. Li, *Nat. Commun.*, 2024, **15**, 3050.
94 T. Deng, H. Zhao, M. Shi, Y. Qiu, S. Jiang, X. Yang, Y. Zhao and Y. Zhang, *Small*, 2024, **20**, 2404254.
95 D. G. Meeker, S. V. Jenkins, E. K. Miller, K. E. Beenken, A. J. Loughran, A. Powless, T. J. Muldoon, E. I. Galanzha, V. P. Zharov, M. S. Smeltzer and J. Y. Chen, *ACS Infect. Dis.*, 2016, **2**, 241–250.
96 S. Wang, C. Duan, W. Yang, X. Gao, J. Shi, J. Kang, Y. Deng, X. Shi and Z. Chen, *Nanoscale*, 2020, **12**, 17555–17556.
97 Y. Liu, P. Cui, R. Tan and S. Ru, *ACS Omega*, 2024, **9**, 26133–26148.
98 Y. Song, Q. Sun, J. Luo, Y. Kong, B. Pan, J. Zhao, Y. Wang and C. Yu, *Nano-Micro Lett.*, 2022, **14**, 83.
99 A. Frei, A. D. Verderosa, A. G. Elliott, J. Zuegg and M. A. T. Blaskovich, *Nat. Rev. Chem.*, 2023, **7**, 202–224.
100 Z. Chen, T. Feng, J. Shen, J. Karges, C. Jin, Y. Zhao, L. Ji and H. Chao, *Inorg. Chem. Front.*, 2022, **9**, 3034–3046.
101 X. Cao, M. Li, Q. Liu, J. Zhao, X. Lu and J. Wang, *Small*, 2023, **19**, 2303195.
102 Y. Pang, Y. Luo, T. Liu, Q. Li, L. Mei, J. Zhang, C. Li, J. Li and Y. Sun, *Chem. Sci.*, 2025, **16**, 19632–19643.
103 Q. Li, H. Ye, F. Zhao, Y. Li, Z. Zhang, Q. Yan and Y. Sun, *Dalton Trans.*, 2024, **53**, 3434–3444.
104 Y. Li, F. Huang, P. J. Stang and S. Yin, *Acc. Chem. Res.*, 2024, **57**, 1174–1187.
105 S. Wu, M. Wang, Z. Liu and C. Fu, *Microorganisms*, 2025, **13**, 1570.
106 M. Claudel, J. V. Schwarte and K. M. Fromm, *Chemistry*, 2020, **2**, 849–899.
107 F. Chen, Y. Li, X. J. Lin, H. Qiu and S. Yin, *Polymers*, 2021, **13**, 370.
108 H. Chen, Y. Song, Y. Peng, M. Wang, W. Dessie, G. J. Duns, L. Xu, X. Luo and Z. Qin, *Macromol. Biosci.*, 2023, **23**, 2200514.
109 Q. Jia, Z. Fu, Y. Li, Z. Kang, Y. Wu, Z. Ru, Y. Peng, Y. Huang, Y. Luo, W. Y. Li, Y. Hu, X. Sun, J. Wang, Z. Deng, C. Wu, Y. Wang and X. Yang, *ACS Appl. Mater. Interfaces*, 2024, **16**, 13422–13438.
110 J. Liu, Y. Wang, W. Gao, M. Cao, H. J. Bian, S. Wang, L. Gui, C. Zhao, Y. Gu, Q. Zhong, J. Zheng, L. Zhang and Z. Yuan, *Adv. Funct. Mater.*, 2025, **35**, 2411986.

